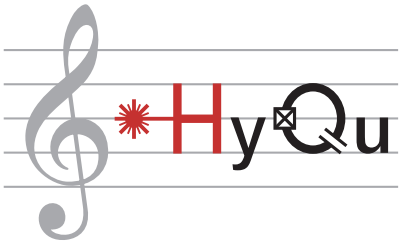

Characterization of locking schemes for cavity bulk optomechanics

Quantum Engineering MSc Semester Project

Unit: Hybrid Quantum Systems Group
D-PHYS, ETH Zurich

Supervisors: Tom Schatteburg
Prof. Yiwen Chu

Author: Emre Yazici
f.emre.yazici@gmail.com

May 2022

1 Introduction

Optomechanical systems (OMS) are those that involve coupling between mechanical and optical modes via e.g. radiation pressure forces [1]. Study of these systems has brought into light numerous advances in quantum sensing, communication and information processing [2]–[5]. Optomechanics continues to be a promising platform for further progress in these fields.

Implementation of sophisticated quantum protocols using OMS requires robust quantum control of phonons [6]. A proposal to achieve this goal is through efficient coupling to bulk acoustic waves within a macroscopic solid by placing it inside a Fabry-Pérot resonator. Relatively high motional masses and access to high-frequency phonon modes in the crystalline solid lead to desirable characteristics for this purpose. Appreciable coupling strength and larger than unity cooperativity has been shown in such a system involving high frequency (13 GHz) phonons mediating resonant coupling between two distinct optical modes via Brillouin interactions [7]. In the same work, it is also demonstrated how the presence of reflective interfaces in an optical cavity changes its spectrum. Particularly, its free spectral range (FSR) becomes a function of the relevant optical mode frequencies as well as the distance between the cavity mirrors and the position of the crystal. Our experimental setup includes such a resonator with a crystal (quartz) fixed between the mirrors. The ensemble is then placed inside a dilution refrigerator capable of cooling the ensemble down to mK temperatures, hence the name *cryo-cavity*.

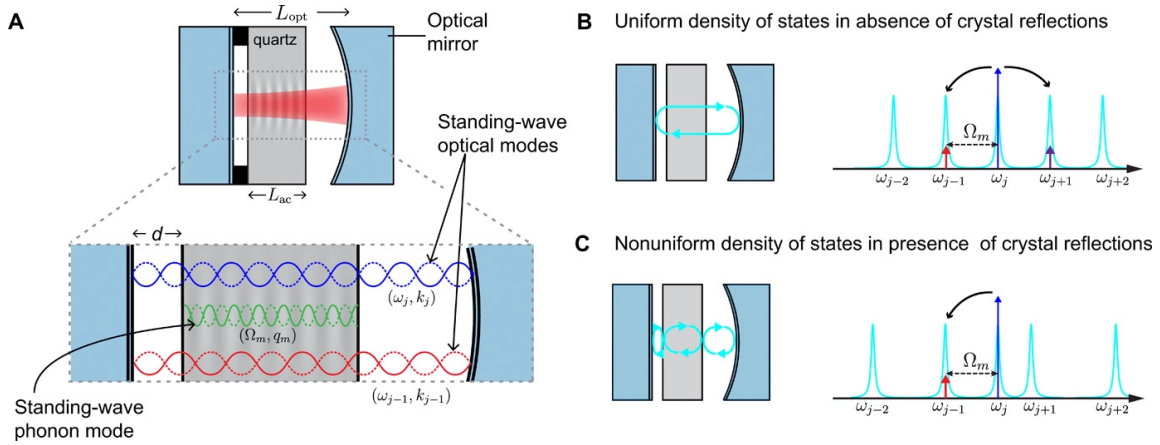

Figure 1: Optical cavity with a crystal inside (A), optical mode spectrum without considering reflection at crystal surfaces (B) and modulation of said spectrum when reflections are included (C). Figure taken from Reference [7].

In order to drive a Fabry-Pérot resonator at desired laser frequencies, one must ensure that noise in either the laser or the cavity does not push the system out of resonance. An effective and commonly used approach for this is the Pound-Drever-Hall frequency stabilization (PDH) [8]. The PDH technique works by the modulating the phase of the incoming laser beam and mixing the reflected cavity light with the same local oscillator to generate the PDH error signal. The error signal obtained in this way will then be linear around the minima of reflection, corresponding to cavity resonances in the optical spectrum. Well understood and extensively studied tools of linear control theory, such as a PID controller, can then be used to stabilise the laser frequency [9]. As stated in a previous work on this topic [10], for the purposes of our measurements it is sufficient to establish an error signal similar to that in Figure 2 for successfully implementing PID control with the PDH technique.

Coherent control of vibrational modes inside the crystal involves short laser pulses to drive Brillouin-scattering induced interactions between the optical and the mechanical modes [7].

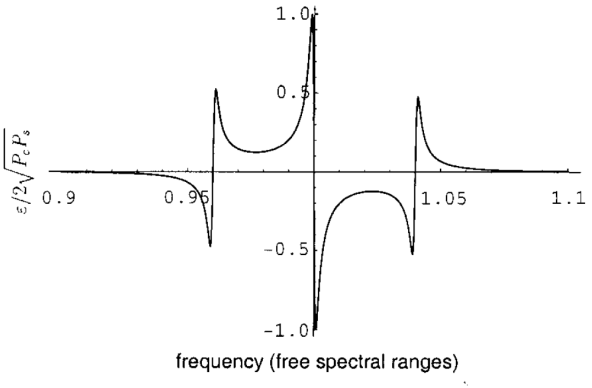

Figure 2: PDH error signal in the regime where the modulation frequency is high and the response around a cavity resonance is linear with a steep slope. Figure taken from Reference [8].

However, the PDH technique, and consequently the lock between the laser frequency and one of the cavity modes, requires a continuous reflection signal. Therefore, if the laser is turned off for some time one risks that noise in the system shifts the cavity out of resonance with the set laser frequency during the interval before the pulse is sent. In this work, we study how to overcome this complication by characterizing two different locking schemes.

First, we will consider if the noise in our experimental setup does drive the cavity out of resonance with the laser in the typical time scales involved. In a similar work, this loss of PDH feedback for a short time before sending in the pulse was not found to be a limitation [11]. Since it can be seen as using the durability in time of the frequency lock point, we call this scheme *Lock Stability*.

In order to implement the PDH technique, we can make use of a laser sideband resonant with a cavity mode that does not take part in the optomechanical interaction. This way, we can use two optical modes that are separated by the Brillouin frequency of quartz for the pulse experiment and a third mode for the PDH lock. As long as the spacing between these modes does not change strongly in time scales involved, all three tones will be resonant with the optical modes if one of them is. For a detailed discussion on such *displacement insensitive* modes, please refer to Reference [10]. For the purposes of this work, it is sufficient to note that for an appropriately chosen cavity mode j, modes $(j-1, j, j+2)$ form a trio of displacement insensitive modes. This approach constitutes what we refer to as *Sideband Locking*.

In the scope of this report, we characterize the discussed locking schemes by analyzing what percentage of input power is reflected from the cavity when they are implemented. This provides a measure of the resonance between the laser and the cavity and thus of the effectiveness of the proposed schemes.

2 Experiments and Results

In this section, we will present the measurements taken in the scope of this project as well as the result that we obtained. As mentioned before, we have characterized two different locking schemes: lock stability and sideband locking. Lock stability involves using the relatively slow drift in cavity frequency to ensure that the laser is resonant with the relevant cavity mode for some time after the PDH error signal, and active stabilization, is lost. Sideband lock on the other hand hinges on the presence of displacement insensitive modes that can be used to obtain an error signal without exciting the relevant science mode(s).

For both lock schemes, we have conducted experiments to measure and analyze the frequency-lock quality between the laser and the cavity. We report these results in form of percent reflection time traces that are obtained by taking the average of many samples at each time point. This corresponds to an expected reflection percentage while the standard deviation at each point reveals the variance in our data set, in other words how significant *outliers* (such as large deviations from resonance) we have at that point.

Since the cryo-cavity sits inside a dilution refrigerator, it suffers from additional sources of noise compared to similar resonators that e.g. sit on top of an optical table. In particular, the pulse tube (PT) introduces strong periodic vibrations that prevent establishment of a lock between the laser and the cavity and thus needs to be turned off during the measurements.

2.1 Lock Stability

Given the relatively short time scales involved, it may be the case that the frequency of the cryo-cavity mode stays stable during the delay between turning the continuous laser off and performing the pulsed experiment. This essentially corresponds to locking the laser to resonance with the cavity and losing the PDH error signal, and by extension PID stabilization of the laser frequency for some time before sending in the pulse.

Our aim in this part is to characterize the deviation in the optical power inside the cavity once the active feedback by the PDH lock is turned off by measuring the optical power reflected back to the input port. We achieve this by taking snapshots of the output voltage of a photodetector monitoring the reflected power, synchronized to the moment the active feedback by the PDH lock is off. We will now give a detailed account of the measurement setup, as well as the procedure followed to find the results we got.

2.1.1 Measurement Setup

A tunable laser, with an associated laser controller, produces the light tone that we use during our measurements. The frequency of the laser is controlled by a stepper motor that changes the wavelength of the laser in steps of 8pm and a piezoelectric motor that modulates it a relatively small amount ($\sim$ 35GHz) around the set value. It is the piezo-motor that implements the PDH locking scheme, driven by feeding the error signal to the integrated PID controller of the laser controller.

The gain parameters of the PID controller are tuned by observing the lock quality and optimising them based on these observations. Depending on the optical power level that we decide to use during our measurement, the PDH error signal strength changes. Since the stabilization of the laser frequency depends on this signal, the overall gain of the PID controller must be adjusted to compensate any changes. Within the linear regime of the components used to implement the PDH lock, this adjustment will be inversely proportional to the change in power level with respect to the previously found optimum. For example, a change of -3dB in optical power will lead to doubling of the PID overall gain. For the following measurements, the values in Table 1, found in previous similar measurements, was used as reference.

Power at 10% detector	-19 dBm
PID2 - Overall gain	2.4
PID2 - P gain	0.03
PID2 - I gain	15.03
PID2 - D gain	23.31

Table 1: Reference values used for setting the PID2 controller gains for the lock stability measurements.

As mentioned before, PDH technique relies on weak modulation of the main tone to generate the error signal. To realize this, we use a phase modulator (PM) after the laser in our setup. It is driven in the 40-50MHz range by a radio frequency signal generator. The amplitude of the RF drive determines the power in the modulated PDH sidebands while the frequency determines the shape of the error signal.

We make use of a electrically controllable variable optical attenuator (VOA) to reduce the optical power in our setup to the desired level. The DC bias voltage is supplied by a lab-type DC source.

The optical power in the system is monitored by a photodetector inserted after the VOA on a 90/10 beamsplitter. The crystal inside our cavity has birefringent properties. Therefore the polarization of the incident light is important. For this reason, we have a fiber polarization controller in our setup.

The final component before the dilution refrigerator is a circulator placed to separate the input line to the cavity (port 1) from the returning light that's reflected from the cavity (port 3). We tune the polarization by looking at the cavity reflection spectrum and optimising it such that only the resonance dip corresponding to the relevant mode is visible.

A photodetector in turn measures the reflected power for implementing the PDH lock. We also make use of a beamsplitter such that the reflected power can be monitored on an oscilloscope by feeding it to another photodetector.

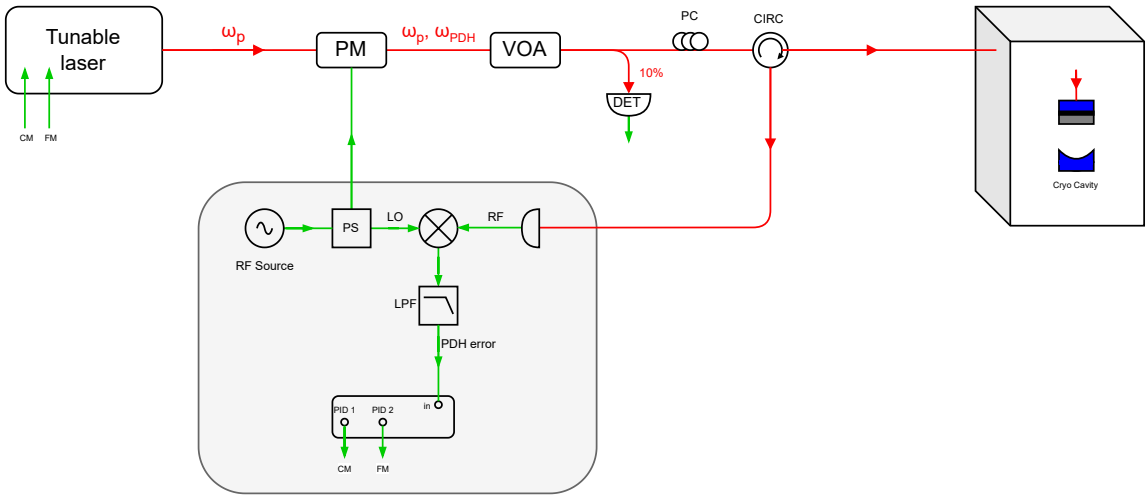

Figure 3: A simplified diagram of the measurement setup. Red lines indicate optical signal propagation and green lines are for RF signals. Shaded region consists of electronics that generate the PDH error signal.

2.1.2 Measurement Procedure

We start preparing for the measurement by, as usual, verifying that all the components and fibers are connected properly. Once we set the optical power level going to the cavity, we adjust the laser controller PID gain. The next step is to prepare for data acquisition by setting up the oscilloscope channels that are used for the reflection signal and trigger; while making sure that the sampling rate and window time is appropriate for the measurement (80MS/s and 20ms in our case). Afterwards, the RF signal driving PDH phase modulator must be optimised as well as the polarization of light. Once all these preparation steps are done, we can turn the pulse tube of the dilution refrigerator off.

The measurement starts with turning the PDH lock on and waiting for some time to make sure the lock is stable. Once it is stable, we send the *lock hold* command to the laser controller and it will give out a trigger signal once the lock is on hold. The oscilloscope, synchronised to this trigger, in turn captures a time trace of the cavity reflection signal. It is imperative that during these measurements the dilution fridge pressure and temperature are monitored closely as they will both rise due to the PT being off. As soon as we finish the measurements, we turn the PT back on and store the data for analysis.

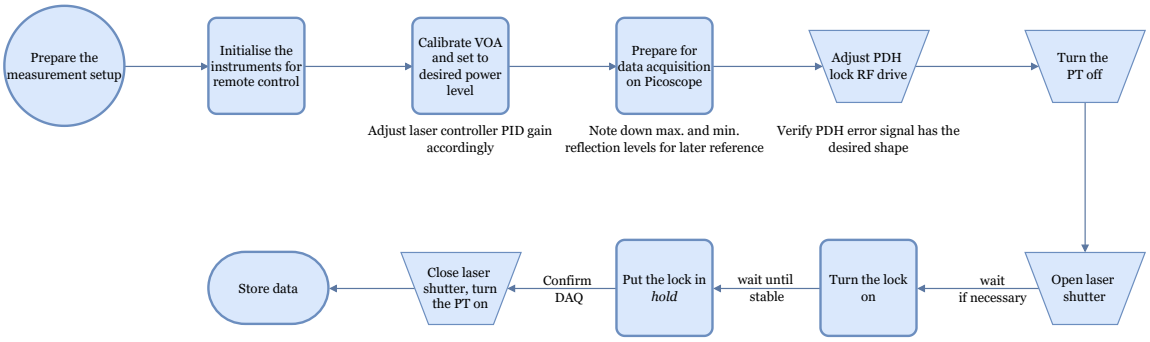

Figure 4: A simplified diagram of the measurement flow.

2.1.3 Results

In order to have an assessment of how long the laser stays on resonance without active feedback, a sensible choice is to compare the reflected power from the cavity when the PDH lock is on to immediately after it is put on hold. For this, we captured a time-trace of the reflected optical power as measured in the photodetector symmetrically around the trigger from the laser controller that indicates the laser PID controller is on hold.

We stress once more that the lock being set to hold is functionally the same as its being off, in the sense that there is no longer an active feedback stabilizing the laser frequency to the cavity mode. However, if we turn the lock *off* on the laser controller, it relaxes the piezo-motor back to its position before the lock was engaged, resulting in immediate detuning of the laser from the cavity. That's why we use the *hold* command. This way, the piezo-motor stays at its last position and we can observe how much the cavity shifts out of resonance in time.

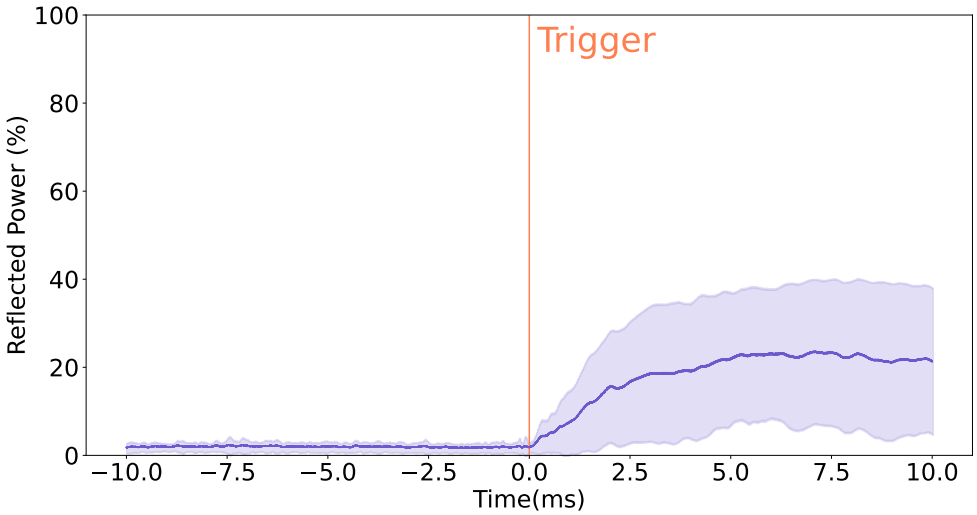

Figure 5: Percentage of reflected optical power, as measured from the input fiber port of the cryo-cavity (T = 4K). Orange line marks the instant the laser controller sends a trigger to indicate the lock is in *hold* position. Trace obtained by averaging 50 different samples taken in the same day. Shaded region indicates one standard deviation around the mean values.

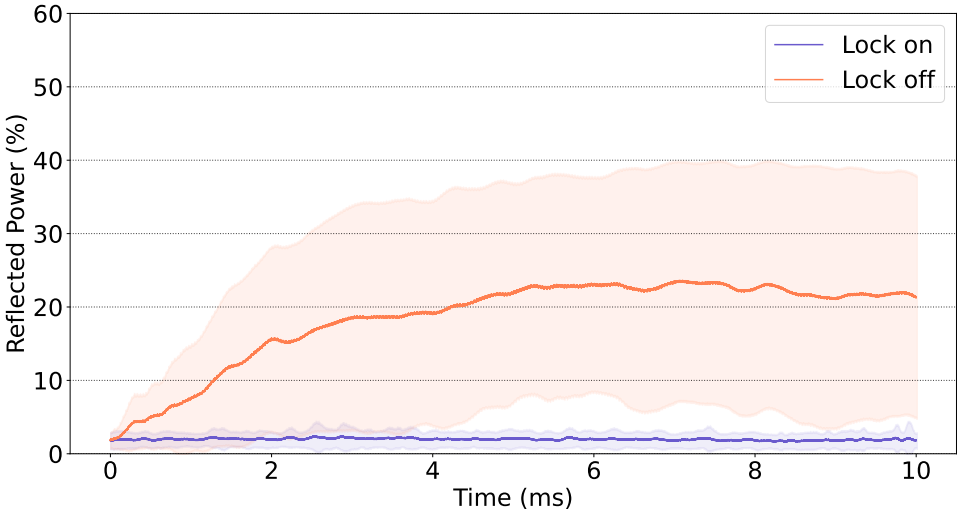

Figure 6: Same as Figure 5 with the two halves superimposed. While the lock is on, the resonance between the laser and the cavity varies little with time. If there is no active feedback, however, the resonance gets noticeably worse in millisecond time scales.

As can be seen on the figures 5 and 6, the PDH locking scheme works as expected and keeps the reflected power percentage to $1.98 \pm 1.6\%$ when engaged. As soon as the active feedback is suppressed, the laser is no longer following the variation in the cavity mode frequency and we observe a gradual shift out of resonance. In 1 ms, the reflected optical power gets as high as 7.5% of the input power. In around 4ms, it reaches 20% and stays around this value for the remainder of our measurement window. Considering that optomechanical coupling strength scales with the square root of the intracavity photon number [6], [7], 20% reflection at the cavity would correspond to 10.6% weaker coupling.

Time after trigger	**Reflected Power (%)**	**Standard Deviation**
0.5 ms	5	5.82
1 ms	7.5	9.89
1.5 ms	12	14.74
2 ms	16	17.24

Table 2: Mean reflected power percentage and its standard deviation at selected points in time after the lock is turned off.

These results are inline with our expectations that the numerous noise sources present in the cryo-cavity environment will cause a drift in the cavity frequency which, if not compensated for in the laser controller, will result in loss of resonance between the laser and the cavity. Saturation at around 20% reflection for the timescales involved points to a harmonic noise source which causes the cavity frequency to oscillate around its previous value. In longer timescales, the slow drift of the cavity frequency becomes significant and results in a total loss of resonance between the laser and the cavity.

The variability in the resonance quality, here quantified by the standard deviation, grows rapidly as well, reaching 24% at its maximum and 9.9% at the 1ms mark. This value is higher than the mean at the same point. From this, we can infer that in some instances of our data set the reflected power is significantly higher than most others. Inspecting the figures in Appendix B we can see that this is indeed the case.

Inspecting figures 7 and 8, we see that the PDH lock lowers the noise floor considerably in the lower frequencies and to some degree in the whole spectrum shown here. Distinct peaks in the no-feedback control case are suppressed and show a broadened comb-like signature. We observe this primarily in the peaks around 28.2kHz and its higher harmonics.

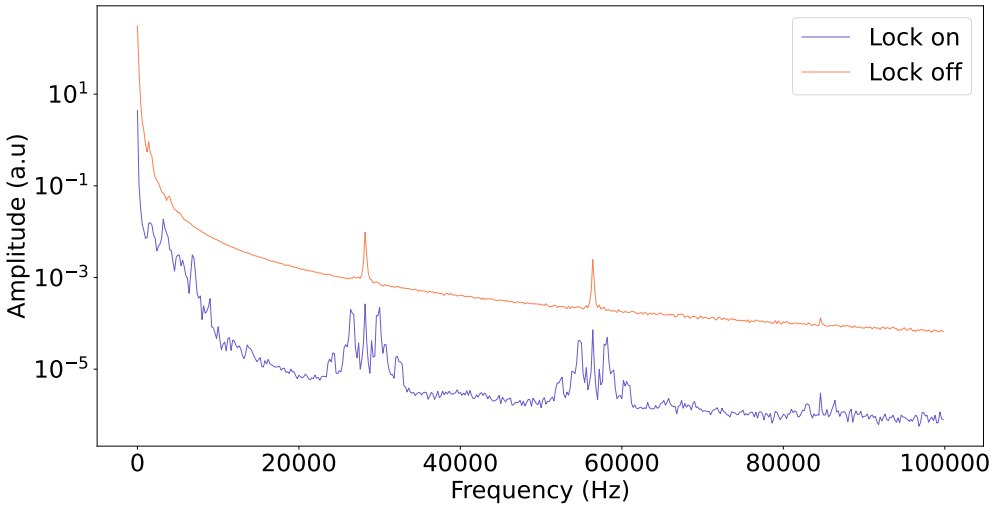

Figure 7: Power spectral density of the reflection percentage. Trace obtained by averaging the PSD of 50 different samples taken in the same day.

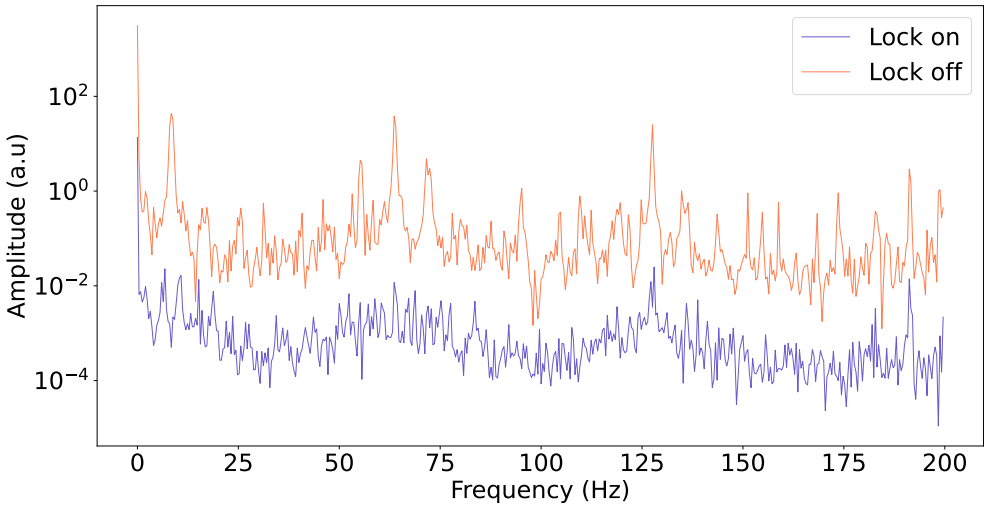

Figure 8: Power spectral density of a longer window measurement taken to analyse sub-kHz frequencies. The PDH lock behaves similarly in this range as well and attenuates the noise considerably.

We also include here results of the same measurement taken on a free space Fabry-Pérot resonator sitting on an optical table. The resonator being isolated from vibrations as well as the lack of additional noise sources that are present in the dilution refrigerator result in a much less important drift in cavity mode frequency compared to the cryo-cavity. This results in significantly lower reflected power percentages as can be seen on Figure 9.

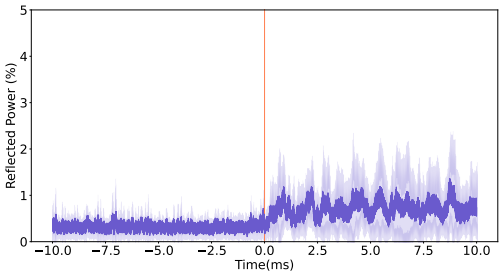

Figure 9: Percentage of reflected optical power, as measured from the input fiber port of the free space cavity. Orange line marks the instant the laser controller sends a trigger to indicate the lock is in *hold* position. Trace obtained by averaging 8 different samples. Shaded region indicates one standard deviation around the mean values.

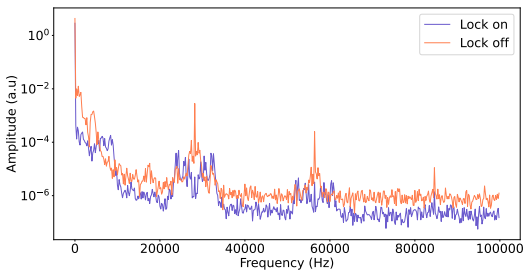

Figure 10: Power spectral density comparison for the free-space cavity. We see that when the lock is engaged, the noise floor is lower across the spectrum. Distinct noise peaks are replaced with suppressed peaks at the edges consistent with a filtering action.

We notice the same 28.2kHz noise here as well. The exact source of this noise, or whether it is an artifact e.g. due to the electronics used, is beyond the scope of this work, especially since its amplitude is less significant than the low frequency noise in our system.

2.2 Sideband Locking

In a previous work [10], it was shown that for our cryo-cavity, modes $(j, j-1)$ and $(j, j+2)$ are relatively *displacement insensitive* for an appropriate choice of j. Particularly, if the cavity FSRs can be tuned in situ such that the Brillouin frequency matched mode pair $(j, j-1)$ sits at a local maximum of FSRs, then the first red mode $(j-1)$ and the second blue mode $(j+2)$ frequencies are similarly affected by cavity length fluctuations relative to (j). This means they will shift by approximately the same amount for the same vibrational noise. Then, if our laser is resonant with one of these modes, and if we know the exact FSR of our cavity, we can modulate the laser to generate sidebands which are expected to be resonant with the two other modes. This is the essence of what we refer to in this work as *Sideband Locking*.

To characterize the sideband locking scheme, we measure the reflected optical power from the cavity and analyze if the additional presence of $(j-1)$ or $(j+2)$ tones affect the reflected power percentage. Since only the main tone is locked to the cavity with the PDH technique, we expect that the other tone will stay in resonance if and only if it is displacement insensitive with respect to the main tone. If it drifts out of resonance, this should be clearly visible as an increase in reflected power. In order to realise this, we send two such tones to the cryo-cavity and capture a time trace of the reflected optical power using a photodetector.

2.2.1 Measurement Setup

The measurement setup for characterizing the sideband locking scheme consists of a main arm that's similar to the one used for lock stability and a sideband arm.

The laser as well as the PDH electronics are the same as in the lock stability measurements and the relevant features were explained in Section 2.1.1.

For the following measurements, the values in Table 3, obtained by optimising the lock by observing the mean and standard deviation of the error signal, was used as reference PID gains.

Power at final BS detector	-20 dBm
PID2 - Overall gain	13.6
PID2 - P gain	0.03
PID2 - I gain	15.03
PID2 - D gain	23.31

Table 3: Reference values used for setting the PID2 controller gains for the sideband lock measurements.

Right after the laser, there is a 50/50 beamsplitter that separates the main arm and the sideband arm. The main arm is essentially consists of a phase modulator that is used to imprint the PDH modulation and a VOA to control the optical power. After going through a polarization controller it is recombined with the sideband arm at the final beamsplitter.

The sideband arm incorporates a single sideband modulator (SSBM) and the related electronics to generate the second light tone we use in our experiments. The SSBM bias controller sets the bias voltages that determine which sideband(s) the SSBM generate. It can be monitored and configured via the associated software on a PC. The RF wave generator sets the frequency by which the light tone is modulated. The output power in the sideband depend on the input laser power but it can also be limited by the available RF power. Like the main arm, we make use of a VOA to adjust the optical power in the sideband arm and a polarization controller to optimise the polarization for the right dip as seen on the reflection spectrum.

The light tones in the two arms are then recombined in a beamsplitter and sent to the cryo-cavity after passing through a circulator. The reflected light coming from the cavity is directed by the circulator (port 3) to the PDH electronics to generate the error signal and to a separate photodetector connected to an oscilloscope. It is the voltage read on this oscilloscope that we use as a measure of reflected power.

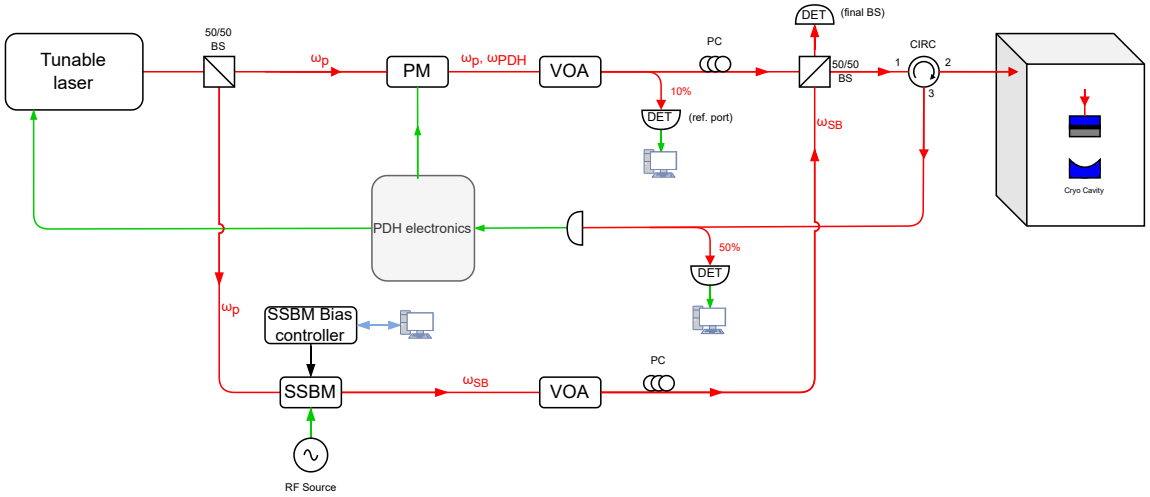

Figure 11: A simplified diagram of the measurement setup. Red lines indicate optical signal propagation and green lines are for RF signals.

2.2.2 Measurement Procedure

We start preparing for the measurement by, as usual, verifying that all the components and fibers are connected properly. We can then set the laser to the desired mode by setting the wavelength and the piezo offset and start emission (with the shutter still closed). Once the laser is on we configure the VOAs in both arms to strongly attenuate the light and open the laser shutter. The next step is to prepare for data acquisition by setting up the channel that are used for the reflection signal. We make sure that the sampling rate and window time is appropriate for the measurement. Afterwards, the RF signal driving PDH phase modulator must be optimised as well as the polarization of light. Next, we turn on the RF generator for the SSBM and let the bias controller find an optimum. If it cannot find a lock point, it may be necessary to restart its scan until the correct bias voltages are set. We can then set the optical power by first closing off the sideband VOA completely and adjusting main arm VOA to get a reading of 3dB below the desired value on the final beamsplitter. The sideband arm VOA can the be tuned until the desired total power level is reached. This procedure will result in an approximately equal distribution of power in the light sent to the cavity between the main frequency and the sideband.

Once all these preparation steps are done, we can turn the pulse tube of the dilution refrigerator off.

The measurement starts with turning the PDH lock on and waiting for some time to make sure the lock is stable. At this point, it may be necessary to try several different sideband frequencies around the rough FSR estimate, that we can get e.g. by visually optimising the dip by looking at the reflection spectrum, to make sure that the sideband sits exactly on the intended cavity mode. We have found empirically that an accuracy of 10kHz is sufficient for this. Further adjustments don't lead to a noticeable difference for our measurements, which is not surprising since the cavity modes that we use have linewidths around 3MHz.

Having made sure that all parameters are set correctly, we can then start data acquisition. It is imperative that during these measurements the dilution fridge pressure and temperature are monitored closely as they will both rise due to the PT being off. As soon as we finish the measurements, we turn the PT back on, stop the lock and store the data for analysis.

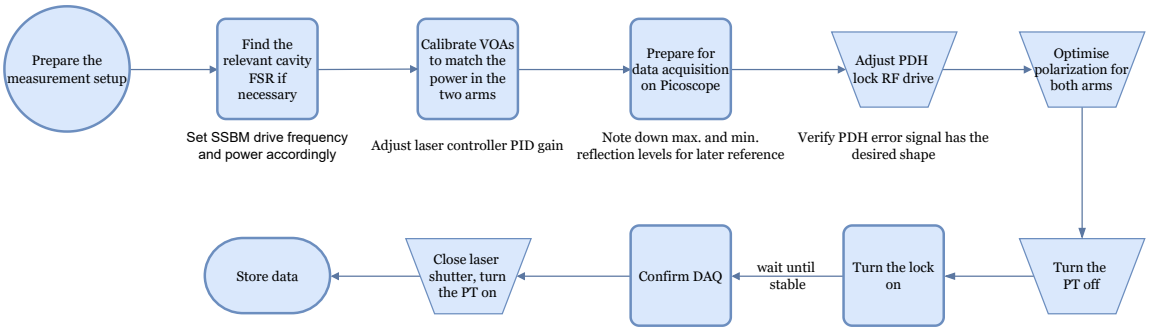

Figure 12: A simplified diagram of the measurement procedure for the sideband locking scheme.

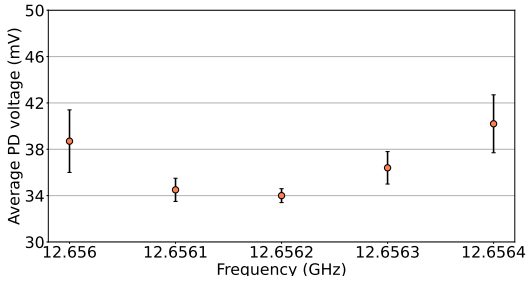

Figure 13: Tuning the FSR for the first mode pair: average reflected power as a function of the sideband frequency.

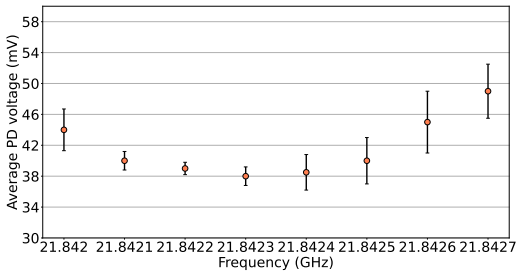

Figure 14: Same graph for the second mode pair used for the measurements.

2.2.3 Results

We use the percentage of the input power reflected from the cavity as a measure of resonance between the light tones and the cavity modes. This can be characterized by capturing a time trace of the reflection photodetector output voltage (circulator port 3).

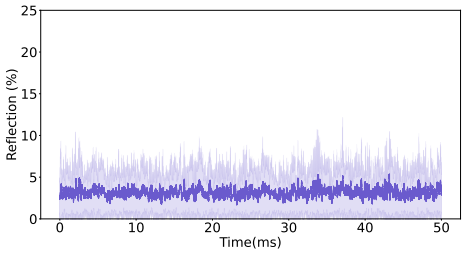

Figure 15: Baseline measurement where only the tone of light used for the PDH lock (j) is present. The cavity temperature was around 80mK and the power measured at the final BS powermeter was -20.06dBm. Graph obtained by taking the average of 32 separate traces. Shaded region corresponds to one standard deviation around the mean value.

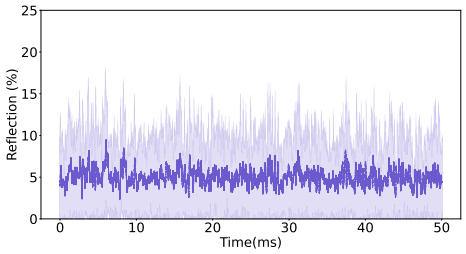

Figure 16: 1 FSR spanning measurement where two tones of light corresponding to modes $(j, j-1)$ are present. The cavity temperature was around 60mK and the power measured at the final BS powermeter was -20.07dBm. Graph obtained by taking the average of 32 separate traces. Shaded region corresponds to one standard deviation around the mean value.

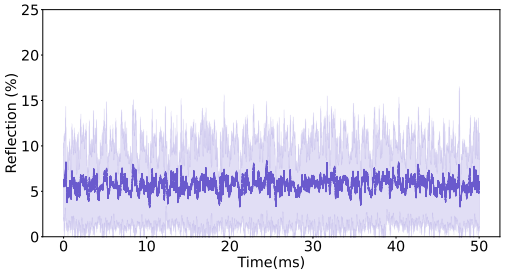

Figure 17: 2 FSR spanning measurement where two tones of light corresponding to modes $(j, j+2)$ are present. The cavity temperature was around 60mK and the power measured at the final BS powermeter was -20.07dBm. Graph obtained by taking the average of 32 separate traces. Shaded region corresponds to one standard deviation around the mean value.

We can see from the figures that reflected power percentage is lower in the baseline measurement when only the main mode is present than the other two measurements with power-matched sidebands. This is in line with our expectations as the sideband tones are not actively locked to the cavity but rely on the displacement insensitivity of the cavity FSR. Even though with such appropriately selected modes the cavity FSR has a particularly weak dependence on displacement, it's not completely independent and this shows up in our data as higher mean and standard deviation in reflected power. That being said, for both mode pairs considered in our measurements the reflected power is around 5% on average. This is low enough that we can thus consider these measurements as an experimental confirmation of the predictions made in the previous work on this topic. [10]

	Baseline	**1FSR**	**2FSR**
Mean Reflected Power (%)	3	5	5
Mean Standard Deviation	2.89	5.18	4.70

Table 4: Mean reflected power and standard deviation of reflection percentage obtained by averaging all the values across different samples for each mode pair.

We also include power spectral densities of the reflection signal for each case reported above. Note the presence of the 28.2kHz noise peak and higher harmonics. Contrary to the lock stability measurements, the harmonic at 56.4kHz is much stronger than the others. This leads us to suspect that it is due to an external source that's not related to our experiment.

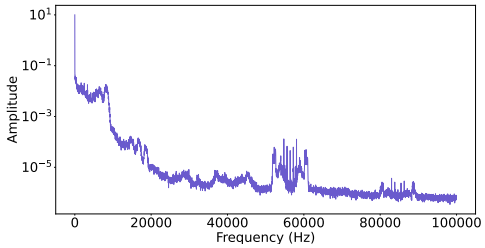

Figure 18: Baseline measurement where only the tone of light used for the PDH lock (j) is present. The cavity temperature was around 80mK and the power measured at the final BS powermeter was -20.06dBm. Graph obtained by taking the average of 32 separate traces.

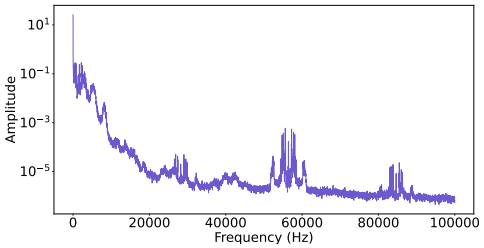

Figure 19: 1 FSR spanning measurement where two tones of light corresponding to modes $(j, j-1)$ are present. The cavity temperature was around 60mK and the power measured at the final BS powermeter was -20.07dBm. Graph obtained by taking the average of 32 separate traces.

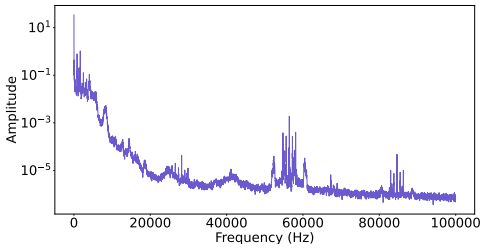

Figure 20: 2 FSR spanning measurement where two tones of light corresponding to modes $(j, j+2)$ are present. The cavity temperature was around 60mK and the power measured at the final BS powermeter was -20.07dBm. Graph obtained by taking the average of 32 separate traces.

3 Conclusions

In this work, we have reported measurements evaluating the effectiveness of two different schemes, *lock stability* and *sideband locking*, in ensuring resonance between a tunable laser and our cryo-cavity.

Our results show that in the sideband locking scheme, reflection from the cavity is around 5% of input power for both displacement insensitive mode pairs. This corresponds to a slight increase compared to the baseline case with a single tone (3%). The standard deviation for each time point, which we use as a measure of variability due to e.g. acute noise sources during measurements, shows a similar trend and is approximately equal to the mean reflection values. We can therefore conclude that sideband locking is a viable approach to circumvent the limitations of the conventional PDH technique for pulsed light experiments.

Lock stability measurements show that noise in out setup shifts the cavity up to 20% out of resonance in the time scales involved in typical optomechanics experiments. Furthermore, any disturbance of the cavity mode is not compensated for by readjusting the laser frequency and this shows up in our data as increase in time of the mean reflection and its standard deviation. We can report here that this scheme shows comparable results to sideband lock for up to 0.5ms after the feedback is on hold. After that point, the metrics for lock stability keep getting worse while there is no such temporal dependence for the sideband lock scheme.

References

[1] F. Marquardt and S. M. Girvin, "Optomechanics," *Physics*, vol. 2, p. 40, 2009.

[2] A. Schliesser, G. Anetsberger, R. Rivière, O. Arcizet, and T. J. Kippenberg, "High-sensitivity monitoring of micromechanical vibration using optical whispering gallery mode resonators," *New Journal of Physics*, vol. 10, no. 9, p. 095 015, 2008.

[3] P. Rabl, S. J. Kolkowitz, F. Koppens, J. Harris, P Zoller, and M. D. Lukin, "A quantum spin transducer based on nanoelectromechanical resonator arrays," *Nature Physics*, vol. 6, no. 8, pp. 602–608, 2010.

[4] R. Riedinger, A. Wallucks, I. Marinković, *et al.*, "Remote quantum entanglement between two micromechanical oscillators," *Nature*, vol. 556, no. 7702, pp. 473–477, 2018.

[5] U. von Lüpke, Y. Yang, M. Bild, L. Michaud, M. Fadel, and Y. Chu, "Parity measurement in the strong dispersive regime of circuit quantum acoustodynamics," *Nature Physics*, pp. 1–6, 2022.

[6] M. Aspelmeyer, T. J. Kippenberg, and F. Marquardt, "Cavity optomechanics," *Reviews of Modern Physics*, vol. 86, no. 4, p. 1391, 2014.

[7] P. Kharel, G. I. Harris, E. A. Kittlaus, *et al.*, "High-frequency cavity optomechanics using bulk acoustic phonons," *Science Advances*, vol. 5, no. 4, 2019. DOI: 10.1126/sciadv.aav0582.

[8] E. D. Black, "An introduction to pound–drever–hall laser frequency stabilization," *American journal of physics*, vol. 69, no. 1, pp. 79–87, 2001. DOI: 10.1119/1.1286663.

[9] K. H. Ang, G. Chong, and Y. Li, "Pid control system analysis, design, and technology," *IEEE transactions on control systems technology*, vol. 13, no. 4, pp. 559–576, 2005.

[10] J. N. Hernandez, "Sideband locking for cavity bulk optomechanics," *Semester Thesis in the Hybrid Quantum Systems Group, ETH Zurich*, 2022.

[11] V. Fiore, C. Dong, M. C. Kuzyk, and H. Wang, "Optomechanical light storage in a silica microresonator," *Phys. Rev. A*, vol. 87, p. 023 812, 2 2013. DOI: 10.1103/PhysRevA.87.023812.

Appendix

Data sets evaluated in this work can be found in the group drive under:

- "`9 - data\Cryo cavity project\Galadriel\202203 Cooldown 8\\20220419_LockStability`" for the lock stability measurements.
- "`9 - data\Cryo cavity project\Galadriel\202203 Cooldown 8\\20220425_LockStability`" for the long window lock stability measurements.
- "`9 - data\Cryo cavity project\Galadriel\202203 Cooldown 8\20220523_SidebandLock`" for the sideband locking measurements.

Lock Stability

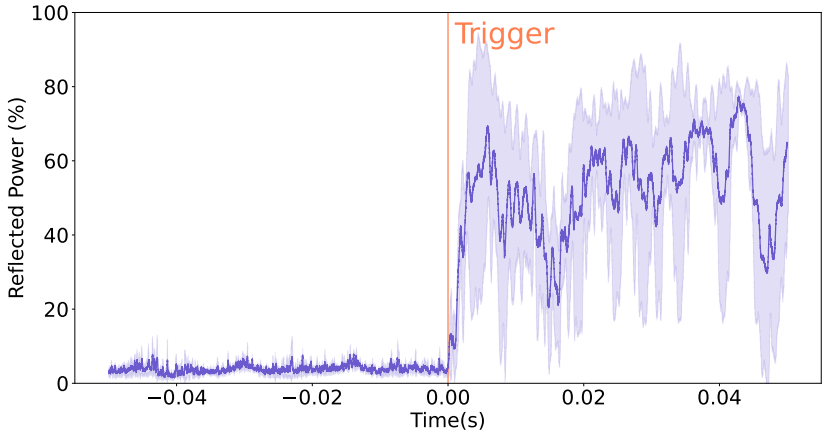

Figure 21: Percentage of reflected optical power, as measured from the input fiber port of the cryo-cavity. Orange line marks the instant the laser controller sends a trigger to indicate the lock is in *hold* position. Shaded region indicates one standard deviation around the mean values. This figure corresponds to the long window measurement that was taken to characterize low frequency noise.

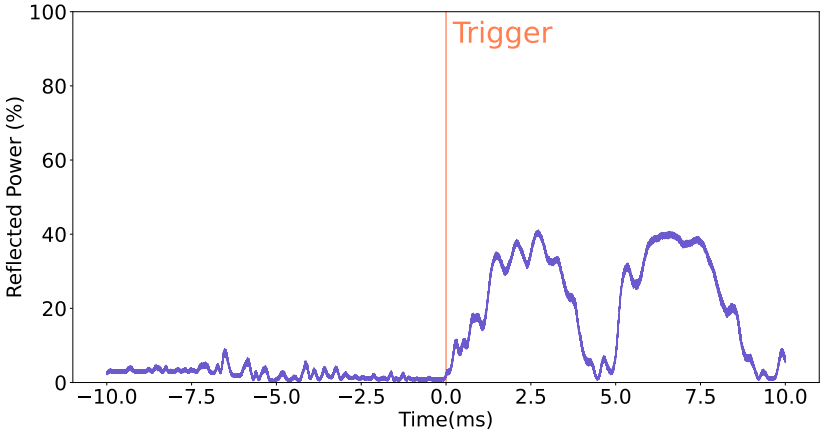

Figure 22: Percentage of reflected optical power, as measured from the input fiber port of the cryo-cavity. Orange line marks the instant the laser controller sends a trigger to indicate the lock is in *hold* position. This trace shows an example of the case when noise in the environment shifts the cavity modes and the reflection quickly increases to as much as 40% of the input optical power. When the PDH lock is engaged (before trigger) there is active feedback and the laser tracks the cavity mode. Note that the shape of the noise is consistent with an oscillation around the cavity resonance, as expected from vibrational noise sources.

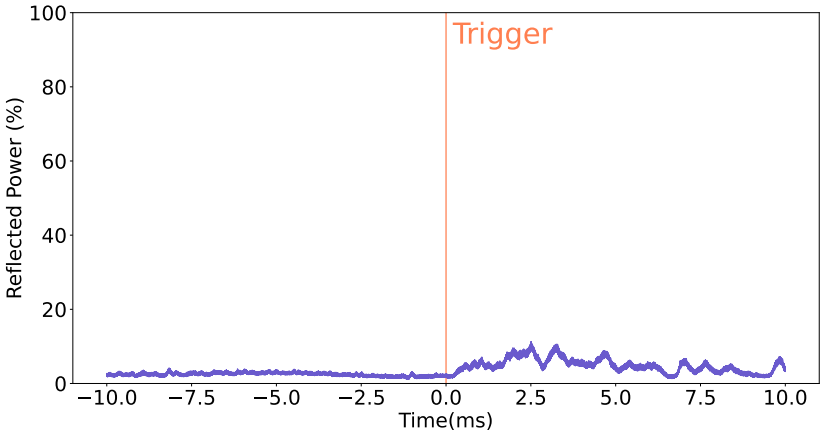

Figure 23: Percentage of reflected optical power, as measured from the input fiber port of the cryo-cavity. Orange line marks the instant the laser controller sends a trigger to indicate the lock is in *hold* position. This trace shows an example where, contrary to Figure 22, there is little noise in the environment and the cavity mode stays at the same frequency for the duration of a typical optomechanics experiment.

Sideband Locking

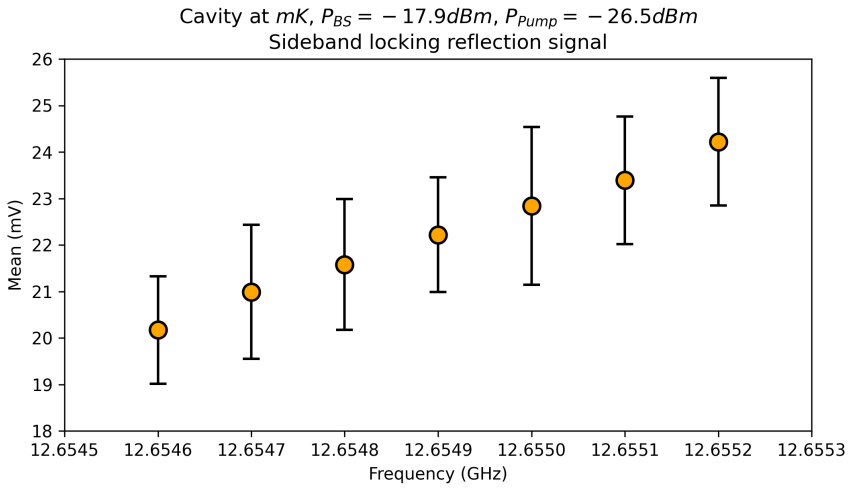

Figure 24: Observed (PD) reflection levels with respect to the laser modulation frequency. As expected, the cavity reflection increases as we go further away from the FSR.

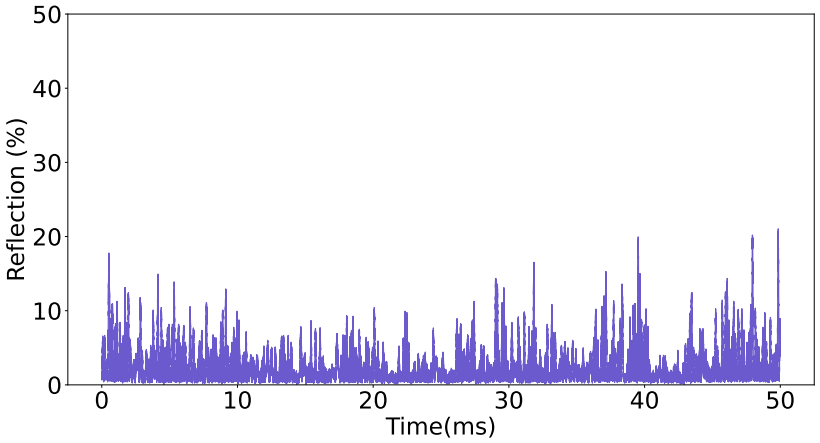

Figure 25: Typical trace obtained for a baseline measurement in the sideband locking scheme.

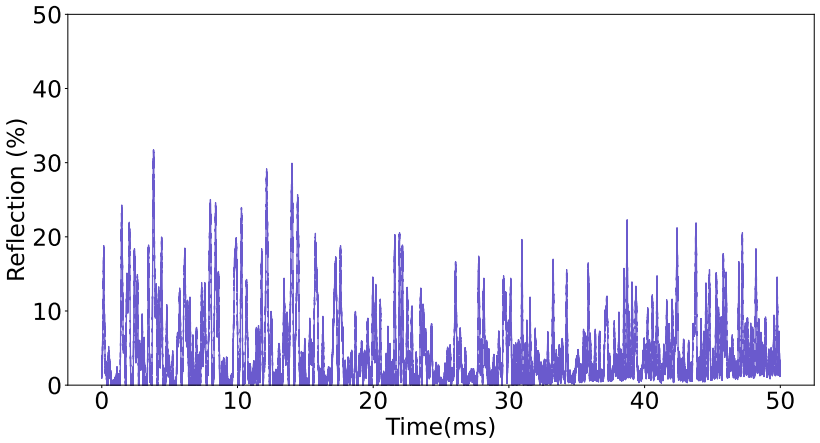

Figure 26: Typical trace obtained for a measurement with $(j, j-1)$ mode pair in the sideband locking scheme. The noise peaks are both higher and more frequent than the baseline but they are quickly suppressed by the PDH control loop.

Acknowledgements

Special thanks to Tom Schatteburg for his excellent guidance during the preparation and execution of the measurements, his input in all phases of this work and always taking time to discuss any questions I might have.

I would also like to express my gratitude towards Prof. Chu for granting me the opportunity to pursue this project and for her leadership that shapes a healthy environment in and out of the lab. Finally, I would like to thank all the members of the Hybrid Quantum Systems Group for their readiness to help whenever I needed it and for making me feel welcome in the group.